Sound Field of a Directional Source in a Reverberant Room

Terence Betlehem and Mark Poletti

Industrial Research Limited, 69 Gracefield Road, Lower Hutt

This paper was previously presented at the 21st Biennial ASNZ Conference, Wellington, NZ

Abstract

It is useful to have an efficient method to determine the sound field in a room produced by a source that is not omnidirectional. A method is thus developed for simulating a "higher order" source with an arbitrary directional pattern in a reverberant room. Several types of directional sources are subsumed by the higher order source, including an arbitrarily vibrating cylinder and an array of vertical line sources arranged on a cylinder. The sound field is calculated by extending the image-source method. For simplicity the sound is modelled in 2-D where sources are either tall or have an infinite vertical extent. A modal expansion of the sound field is used, which reduces the computation of calculating the sound field over a large number of points. The method is particularly suited to array signal processing where the sound field is sampled at multiple points. Efficient algorithms are presented for simulating both circularly-shaped regions absent of sound sources and the entire room.

INTRODUCTION

It is common in room acoustics to simulate the sound field of the omnidirectional source. Yet realistic sources are directional. When the size of a sound source is large in comparison to the acoustic wavelength, it typically creates sound which varies in intensity from one direction to another. Above bass frequencies electrodynamic loudspeakers are directional.

Many sound sources, such as musical instruments also exhibit a natural directivity [1, ch. 4]. It is of advantage in sound reproduction applications to use loudspeakers with directional characteristics. Sound can be directed for example using dipoles [2] towards the walls to generate room reverberation and create a feeling of ambience, or directed toward the listener using cardioid loudspeakers to create a clearly localisable phantom source. In this paper, an efficient method is proposed for simulating the sound field of a directional source in a room.

Accurate methods of simulating a sound field are based upon the wave equation. Many of these methods work by dividing either the free-space or surfaces of the room into elements. Finite difference time domain (FDTD) methods approximate the time domain wave equation over a spatial grid with a difference equation, a number of which are summarized in [3].

Unfortunately the accuracy suffers from numerical dispersion. The wave equation can also be converted into an integral equation and solved with either the finite element method (FEM) or boundary element method (BEM) [4, 5]. The advantage of element methods over FDTD is that elements can be more densely positioned around intricate geometrical structures like the human pinna [6]. The equivalent source method (ESM) [7], where the scattering environment is replaced with an equivalent set of sources, can also account for cylinder scattering and non-regular room geometries. Each of these methods can be adapted for directional sources in a room by imposing a boundary condition on sound velocity on the surface of the directional source.

An efficient sound field model for the omnidirectional source in a rectangular room is the image-source method [8]. Fractional delay filters were used in [9] to permit a time-domain implementation. In [10], the speed of computation of an acoustic transfer function has been improved by replacing the late reverberant tail, which requires computing thousands of image-sources, with a decaying diffuse noise term. Unfortunately this method fails to account for the correlation in the reverberant tail for closely sampled locations. It is unsuitable for array signal processing applications for which the tail holds relevance.

A more promising method is that of [11], where a multipole expansion was exploited to reduce the computational requirements. A simulator for directional sound sources in the room was implemented by modelling a source using its farfield directivity pattern [12]. However this does not account for the variation of the directivity pattern in the nearfield with distance.

This paper presents an extension of the image-source method to an arbitrary directional source in a 2-D rectangular room. The method is accurate in simulating the soundfield in a room with multiple numbers of vibrating cylinders. A frequency-domain method is presented, where the soundfield can be determined discretely at a number of frequencies. Time-domain simulations over a band of frequency can also be performed by sampling the soundfield at adequate numbers of frequencies.

An outline of the paper is as follows. The original image-source method is described. The higher order source (HOS) is then defined and shown to subsume various cylindrical sound source types, including the vibrating cylinder and source-on-cylinder configurations. The proposed image-source method for directional sources is then formulated. Finally, several types of directional sources in rooms are simulated.

IMAGE-SOURCE METHOD

The reverberant sound field of the line source, the 2-D analogue to the acoustic monopole, can be simulated in a straight-forward manner in a rectangular room using the image-source method [8]. This method is based on geometric acoustics, where the reflection off a surface is modelled by the placing an image-

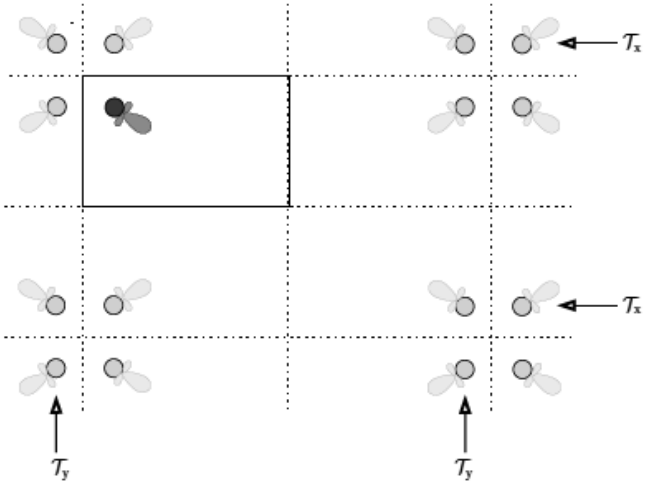

Figure 1. The lattice of image-sources in a rectangular room. Shown is the mirroring of the directivity pattern of each source about the x and y axes which are denoted by transformation T_x and T_y respectively.

source equidistant to the surface on the other side. A lattice of such image-sources is obtained by multiply reflecting the sound source about the walls of the room. The lattice for a rectangular room is depicted in Figure 1.

An expression for the sound field in the room can be written by superposition of image-source sound fields. Following a negative time convention, the sound field in the room created a sound source $\boldsymbol{\ell}$ at angular frequency ω is:

$$P_\ell(\boldsymbol{x};\omega)e^{-i\omega t} = \frac{i}{4}e^{-i\omega t}\sum_{n=1}^{N_{\text{img}}}\xi_n H_0(k\|\boldsymbol{x}-\boldsymbol{y}_{n\ell}\|),$$

where N_{img} is the number of image-source locations, $y_{n\ell}$ is the position of the n^{th} image-source of sound source l, ξ_n is the accumulated reflection coefficient resulting from multiple reflection off the walls corresponding to image-source n [8] and $H_m()$ is the m^{th} order Hankel function of the first kind.

The image-source method can be extended to account for the angular dependence of the reflection coefficient, though this is rarely done in practice. In this paper, the method is extended to simulate the sound field of a solid higher order source. The extension of the image-source method to directional sources is developed below.

SOUND FIELD AROUND A DIRECTIONAL SOURCE

The sound field around an arbitrary directional source $\boldsymbol{\ell}$ with respect to an origin at its centre is:

$$P_\ell(\boldsymbol{x}^{(\ell)},\omega) = \sum_{n=-\infty}^{\infty}\beta_n^{(\ell)}H_n(kr^{(\ell)})e^{in\phi^{(\ell)}}, \quad r^{(\ell)} > r_0, \tag{1}$$

where $\beta^{(\ell)}_n$ is a sound field coefficient, $x^{(\ell)} = (r^{(\ell)};\Phi^{(\ell)})$ is the position in relation to the centre of the source, $H_n()$ is the n^{th} order Hankel function of the first kind and r_0 is a radius bounding the source. The sound velocity of this directional source for a negative time convention is derived from the Euler equation:

$$\boldsymbol{V}_\ell(\boldsymbol{x}^{(\ell)},\omega) = \frac{1}{i\omega\rho}\nabla P_\ell(\boldsymbol{x}^{(\ell)},\omega),$$

where ρ is the density of air and c is the speed of sound in air. Substituting (1) into this expression and applying the gradient rule:

$$\nabla P = \frac{\partial P}{\partial r}\hat{\boldsymbol{e}}_r + \frac{1}{r}\frac{\partial P}{\partial \phi}\hat{\boldsymbol{e}}_\phi,$$

where $\mathbf{e}_r$ is the radial unit vector in the direction of x and $\mathbf{e}_\Phi$ is the tangent unit vector making an angle of $\Phi + \pi = 2$ with the horizontal axis, the velocity vector field at position $x^{(\ell)}$ can be written:

$$V_\ell(\boldsymbol{x}^{(\ell)},\omega) = \frac{1}{ic\rho}\sum_{n=-\infty}^{\infty}\beta_n^{(\ell)}\left[H_n'(kr^{(\ell)})\hat{\boldsymbol{e}}_{r^{(\ell)}} + \frac{in}{kr^{(\ell)}}H_n(kr^{(\ell)})\hat{\boldsymbol{e}}_{\phi^{(\ell)}}\right]e^{in\phi^{(\ell)}}.$$

The sound field shall be computed in a circular region of interest of radius r_c centred about the origin, due to cylindrical sources positioned external to the region of interest in a reverberant room.

The sound fields for several directional sources are summarized below including an arbitrary vibrating cylinder, a line source on a cylinder, an array of line sources on a cylinder.

Sound Field of a Higher Order Source

The sound created by a cylinder vibrating in an arbitrary fashion is now determined, with the goal of deriving the sound field of a source with an arbitrary directivity pattern.

Construct a general height invariant N_a^{th} order directional loudspeaker as a vertical vibrating cylinder of outward-going radial surface velocity $V_l(a,\Phi^{(\ell)})$ at each angle $\Phi^{(\ell)}$. Following [13], the radial velocity may be expressed by the Fourier representation:

$$V_\ell(a,\phi^{(\ell)}) = \sum_{n=-N_a}^{N_a} v_{n\ell} e^{in\phi^{(\ell)}} \qquad (2)$$

where $v_{n\ell}$ is the vibration coefficient of the n^{th} mode of source ℓ and N_a is the order of the sound source.

The radial surface velocity is directly proportional to the pressure gradient on the surface of the cylinder. Adopting a negative time convention, the relation is:

$$V_\ell(a,\phi^{(\ell)}) = \frac{1}{ikc\rho}\frac{\partial}{\partial r^{(\ell)}}\left[P(r^{(\ell)},\phi,\omega)\right]\Big|_{r^{(\ell)}=a}. \quad (3)$$

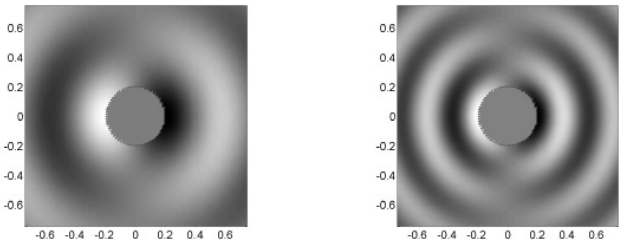

(a) 1st order, 500 Hz (b) 1st order, 1 kHz

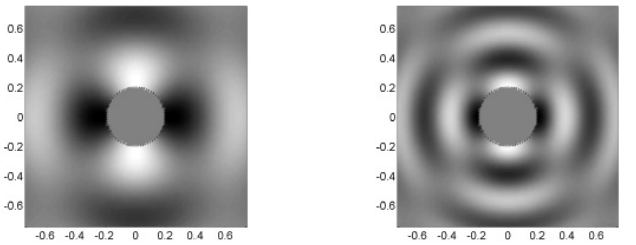

(c) 2nd order, 500 Hz (d) 2nd order, 1 kHz

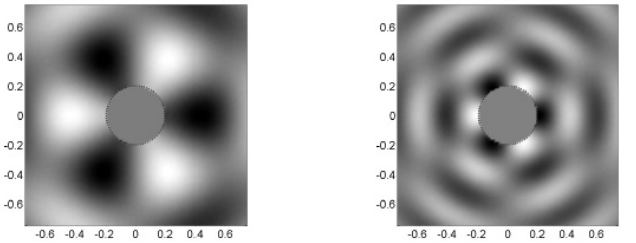

(e) 3rd order, 500 Hz (f) 3rd order, 1 kHz

Figure 2. Modes of vibration of a hard cylinder of radius 0.2m at 500 Hz and 1 kHz. The real part of sound pressure is shown.

Substituting Fourier expansion (2) and directional source expression (1) into (3), and equating each term of the series:

$$v_{n\ell} = \frac{1}{ic\rho}\beta_n^{(\ell)} H_n'(ka). \qquad (4)$$

The sound field around this arbitrary directional source is:

$$P_\ell(\boldsymbol{x}^{(\ell)},\omega) = \sum_{n=-N_a}^{N_a} \underbrace{\frac{ic\rho}{H_n'(ka)} v_{n\ell}}_{\beta_n^{(\ell)}} H_n(kr^{(\ell)}) e^{in\phi^{(\ell)}}, \qquad (5)$$

where the sound field coefficient is underbraced. This equation expresses the sound field as that of a linear sum of higher order sources $H_n(kr^{(\ell)})e^{in\Phi^{(\ell)}}$ each with weighting $v_{n\ell}/H'_n(ka)$ up to the maximum order N. The sound fields of several vibrational modes for a cylinder of radius 0.2m are plotted in Figure 2.

The cylinder modes exhibit an activation property which is dependent on frequency [13]. In Figure 3 the strengths of the cylinder modes $H_n(kr^{(\ell)})/H'_n(ka)$ in the far-field are plotted for all modes active under 1 kHz. A vibrating cylinder of fixed radius has a low order directivity pattern at low frequencies and high order directivity pattern at high frequencies.

The modal response of real loudspeakers may vary. The sound field created by a point source, which is derived below, includes an additional factor of ℓ=k which creates a decay of 20 dB / decade in the modes at high frequencies. Loudspeakers such as electrodynamic loudspeakers include similar frequency dependent factors [1, p. 192].

By operating largely in their mass-controlled region, they produce a sound velocity which varies with the reciprocal of frequency. Due to the radiation impedance of air, this causes the decay at high frequencies.

In the far-field, the sound field can be derived from (5) using the asymptotic expansion of the Hankel function [14]:

$$P_\ell(x^{(\ell)},\omega) \to ic\rho\sqrt{\frac{2}{\pi r^{(\ell)}}} e^{i(kr^{(\ell)}-\pi/4)} \sum_{n=-N_a}^{N_a} \frac{i^{-n} v_{n\ell}}{H_n'(ka)} e^{in\phi^{(\ell)}}$$

The far-field directivity pattern of loudspeaker ℓ at angle Φ is then:

$$D_\ell(\phi) = \sum_{n=-N_a}^{N_a} i^{-n} \frac{v_{n\ell}}{H_n'(ka)} e^{in\phi}.$$

Loudspeaker directivity is a function of both the surface radial velocity controlled by the vibration modes and the cylinder radius which determines the number of active modes.

Sound Field of a Source on a Cylinder

The sound field due to a vertical line source at point $x^{(\ell)}$ about solid cylinder ℓ is [15, 16]:

$$P_\ell(\boldsymbol{x}^{(\ell)},\omega) = \frac{i}{4}\sum_{n=-N}^{N}\left[J_n(kr_s) - \frac{J_n'(ka)}{H_n'(ka)}H_n(kr_s)\right] \times e^{-in\phi_s} H_n(kr^{(\ell)}) e^{in\phi^{(\ell)}}, \quad r^{(\ell)} > r_s$$

for the source positioned at r_s around a cylinder of radius a and $x^{(\ell)}$ is the position in relation to the centre of cylinder ℓ. Due to the high-pass nature of the Bessel functions in order n, the series is allowed to be truncated to $|n| < N = ekr_s/2$ [17].

To determine the sound field of a line source on the cylinder, set $r_s = a$ and apply the Wronskian relation:

$$J_n(x)H_n'(x) - J_n'(x)H_n(x) = \frac{2}{\pi i x},$$

applicable for the Hankel function of the first kind, to obtain:

$$P_\ell(\boldsymbol{x}^{(\ell)}, \omega) = \sum_{n=-N_a}^{N_a} \underbrace{\frac{P_0}{2\pi ka}\frac{e^{-in\phi_s}}{H_n'(ka)}}_{\beta_n^{(\ell)}} H_n(kr^{(\ell)})e^{in\phi^{(\ell)}}, \tag{6}$$

where $N_a = \lfloor eka/2 \rfloor$. The sound field of a line source on a cylinder of radius 0:2m is again plotted in Figure 4.

Sound Field of a Circular Array on Cylinder

Now consider the sound field created by an array of line sources spaced around the surface of cylinder ℓ at polar angles $\{\Phi_1,...,\Phi_p\}$ with source excitation signals $G_{1\ell},...,G_{p\ell}$. The sound field for the circular array of P loudspeakers around solid cylinder ℓ is given by (1) where each sound field coefficient is:

Substituting (7) into (4), the vibrating cylinder mode coefficients

$$\beta_n^{(\ell)} = \frac{P_0}{2\pi ka H_n'(ka)} \sum_{p=1}^{P} G_{p\ell} e^{-in\phi_p}. \tag{7}$$

are:

$$v_{n\ell} = \frac{1}{ic\rho}\frac{P_0}{2\pi ka}\sum_{p=1}^{P} G_{p\ell}e^{-in\phi_p}.$$

A circular array of sources on a cylinder can hence be simulated

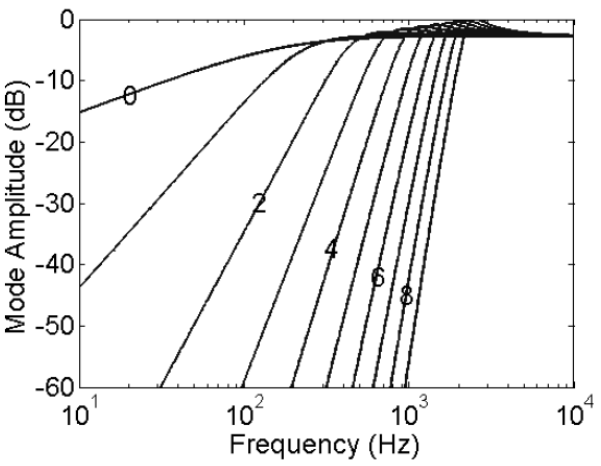

Figure 3. Amplitudes of the modes of vibration for n = 0,...,9 as a function of frequency of a hard cylinder of radius 0.2m.

with an equivalent vibrating cylinder modes $v_{n\ell}$, for $n = -N_a,...,N_a$.

The next section computes the sound field coefficients in a region of interest via a change of origin.

IMAGE METHOD FOR DIRECTIONAL SOURCES

The image-source method for directional sources requires both a translation of a source and a mirroring of a source directivity pattern about a wall. The translation or change of origin method shall be used to derive a computationally efficient method for determining the image-source method in the room. To complete the method, operations shall be defined to mirror the directivity pattern about the x and y axes.

Translation

The sound field in a circular region of interest of radius r centred about a global origin due to a directional source positioned outside the region of interest shall now be determined.

Let the cylinder be at position y_ℓ in a global coordinate system,

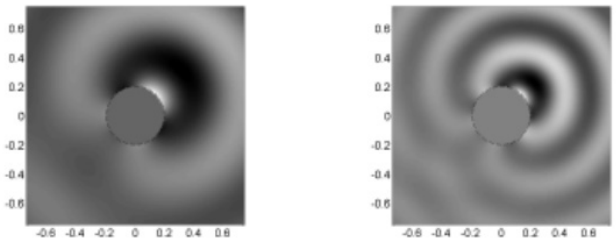

(a) 500 Hz (b) 1 kHz

Figure 4. Line source on a hard cylinder of radius 0.2m positioned at polar angle 45° at 500 Hz and 1 kHz. The real part of sound pressure is shown.

whose origin $\mathcal{O}$ is centred at the region of interest. The sound field around the cylinder is expressed in terms of vector $\mathbf{x}^{(\ell)}$ in reference to origin $\mathcal{O}_\ell$ at the centre of cylinder ℓ. As shown in Figure 5, a change of origin to the global coordinate system is made by writing $\mathbf{x}^{(\ell)} = \mathbf{x}\text{-}\mathbf{y}_\ell$. Using the Bessel function addition formula [18, p. 361], the sound field can be expanded around the global origin:

for $r < R_\ell$ where the series truncation $N_r = ekr_c/2$ is accurate for

$$H_m(kr^{(\ell)})e^{im\phi^{(\ell)}} = \sum_{n=-N_r}^{N_r} H_{n-m}(kR_\ell)e^{-i(n-m)\theta_\ell} \times J_n(kr)e^{in\phi},$$

a region of interest of radius r_c.

Substituting this into (1), the pressure in the region of interest due to directional sound source ℓ is written:

$$P_\ell(\boldsymbol{x},\omega) = \sum_{n=-N_r}^{N_r}\left[\sum_{m=-N_a}^{N_a}\beta_m^{(\ell)}H_{n-m}(kR_\ell) \times e^{-i(n-m)\theta_\ell}\right]J_n(kr)e^{in\phi} \quad (8)$$

for $r < R_\ell a$ or:

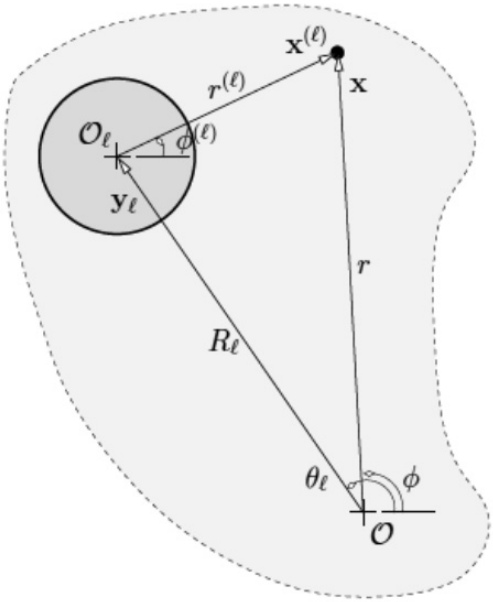

Figure 5: The change of origin for expressing sound pressure around a cylinder with origin $\mathcal{O}_\ell$ in terms of a global coordinate system with origin $\mathcal{O}$.

where $\beta_{n\ell}$ represents the sound field coefficient in the region of interest for loudspeaker ℓ:

$$P_\ell(\boldsymbol{x},\omega) = \sum_{n=-N_r}^{N_r} \beta_{n\ell} J_n(kr) e^{in\phi}, \qquad (9)$$

This equation is a linear convolution of the modes $H_n(kR_\ell)\, e^{-in\Theta l}$ with the sound field coefficients $\beta_n^{(\ell)}$ about the sound source origin $\mathcal{O}_\ell$[2]. A change of origin in 2-D is in essence accomplished by a linear convolution. This is much simpler than in 3-D where translation of basis functions requires the calculation of Clebsh-Gordan coefficients [19, p. 93-122]. The sound velocity vector field in the region of interest for the sound pressure field in (9) is:

$$\beta_{n\ell} = \sum_{m=-N_a}^{N_a} \beta_m^{(\ell)} H_{n-m}(kR_\ell) e^{-i(n-m)\theta_\ell}. \qquad (10)$$

By comparison, the sound field due to a line source located at y in free-space can be expressed [14]:

$$\boldsymbol{V}_\ell(\boldsymbol{x},\omega) = \frac{1}{ic\rho} \sum_{n=-N_r}^{N_r} \beta_{n\ell} \left[J_n'(kr)\hat{\boldsymbol{e}}_r + \frac{in}{kr} J_n(kr)\hat{\boldsymbol{e}}_\phi \right] e^{in\phi}.$$

The sound field coefficient $\beta_{n\ell} = i/4H_n(kR_\ell)e^{-in\Theta l}$ can equivalently be obtained from (10) by setting β_m^{ℓ} to that corresponding to a line source located at $\mathcal{O}_\ell$, i.e.:

$$\frac{i}{4} H_0(k\|\boldsymbol{x}-\boldsymbol{y}_\ell\|) = \frac{i}{4} \sum_{n=-N_r}^{N_r} H_n(kR_\ell) e^{-in\theta_\ell} J_n(kr) e^{in\phi}$$

which helps to validate (10).

$$\beta_m^\ell = \begin{cases} \frac{i}{4}, & m = 0, \\ 0, & m \neq 0. \end{cases}$$

Mirroring

When generating the image-sources for a directional source, the sound field of the directional source must be reflected in addition to the source being translated. This mirroring of image-source directivity patterns are depicted in Figure 1 for the rectangular room.

Assume the axes align with the perpendicular walls of the room. This sound field must then be mirrored about the x and y axes. The reflection of the coefficients $\beta_n^{(\ell)}$ through any combinations of axes shall be represented with a set of transform operators T . The simplest transform to consider is the identity transform, for which $T_1\{\beta_n^{(\ell)}\} = \beta_n^{(\ell)}$. Single axes reflections shall be represented using the operators T_x and T_y.

The transforms used to perform these reflection operations is summarised in Table 1. By way of example, the reflection of the 2-D basis function $H_n(kr^{(\ell)})e^{in\Phi^{(\ell)}}$ about the x axis where $\Phi^{(\ell)}$ tends to $-\Phi^{(\ell)}$ is given by:

$$(-1)^n H_{-n}(kr^{(\ell)}) e^{-n\phi^{(\ell)}}.$$

This result is used to write the transformations that occur on the sound field coefficients:

$$\mathcal{T}_x\{\beta_n^{(\ell)}\} = (-1)^n \beta_{-n}^{(\ell)}.$$

The reflection operators are both commutative: $T_x \circ T_y = T_y \circ T_x$ and self-inverses: $T_x \circ T_x = T_y \circ T_y = T_I$. Because T_x and T_y are self-inverses, mirroring about the x or y axis an even number of times results in an identity operation.

In Figure 1, these properties are shown. The image-sources resulting from reflection off the horizontal (vertical) walls an odd number of times are marked with arrows. The intersection of horizontal and vertically pointing arrows are where image-sources are reflected about both x and y axes ($T_x \circ T_y$). All other image-sources remain unchanged by the wall reflection (T_I). Each image-source hence possesses one of four different sets of sound field coefficients, each derived from the original source coefficients $\beta_n^{(\ell)}$.

Table 1: Transforms to reflect a sound field about the x and/or y axes for loudspeaker l.

Operator	Angle Transform	Coefficient
$\mathcal{T}_x$	$\phi^{(\ell)} \to -\phi^{(\ell)}$	$(-1)^n \beta_{-n}^{(\ell)}$
$\mathcal{T}_y$	$\phi^{(\ell)} \to \pi - \phi^{(\ell)}$	$\beta_{-n}^{(\ell)}$
$\mathcal{T}_x \circ \mathcal{T}_y$	$\phi^{(\ell)} \to \pi + \phi^{(\ell)}$	$(-1)^n \beta_n^{(\ell)}$

Proposed Methods for Directional Sources

The sound field in the room is obtained by summing the sound field contribution from each image-source. The sound pressure at a point in the region of interest due to L cylindrical directional sources at $y_0^{(\ell)} = (R_\ell;\Theta_\ell)$ are determined using one of two methods proposed below.

These methods presume that the lattice of image-source locations $\{y_{n\ell}\}_n$ and corresponding accumulated reflection coefficients $\{\xi_n\}_n$ in the rectangular room for each source ℓ have been pre-computed using the methods in [8]. For simulations, all the images lying within a distance cT_{60} corresponding to propagation distance of one reverberation time from the centre of the room are typically included in the computation. The methods for determining the sound field over the room are:

Algorithm A Without using the change of origin formula, the sound field can be determined directly using an image-source method. For each point of interest **x**, the vector from the origin of each imagesource n of loudspeaker l, $\mathbf{x}^{(\ell,n)}$ $\mathbf{x}$-$\mathbf{y}_{n\ell}$, must be calculated. We write vector $\mathbf{x}^{(\ell,n)}$ in the polar form $(r^{(\ell,n)}, \Phi^{(\ell,n)})$. The sound field must be computed from each image-source at each point in the room using (5):

$$P_\ell(\boldsymbol{x},\omega) = \sum_{n=0}^{N_{\text{img}}} \zeta_n \sum_{m=-N}^{N} \beta_m^{(\ell,n)} H_m(kr^{(\ell,n)}) e^{in\phi^{(\ell,n)}}, \qquad (11)$$

where $\beta_m^{(\ell,n)} = T_n\{\beta_m^{(\ell)}\}$, $T_n\{\}$ is the correct mirroring operator to apply to image-source n and $\beta_m^{(\ell)}$ is obtained from $v_{m\ell}$ using (4).

Algorithm B Using the change of origin formula, the calculation is broken into two steps. In step one, the coefficients of the

sound field in the room are computed:

$$\beta_{m\ell} = \sum_{n=0}^{N_{\text{img}}} \zeta_n \left[H_m(kR_n^{(\ell)}) e^{-im\theta_{n\ell}} * \mathcal{T}_n\{\beta_m^{(\ell)}\} \right], \quad (12)$$

where * is the convolution operator corresponding to change of origin formula (10) and $(R_{n\ell}, \Theta_{n\ell})$ $y_{n\ell}$ is the n^{th} images location of the cylindrical source l. In step two, these coefficients are used to compute the sound field using the interior expansion [14]:

$$P_\ell(\boldsymbol{x}, \omega) = \sum_{m=-N_r}^{N_r} \beta_m J_m(kr) e^{im\phi}, \quad (13)$$

This two-step algorithm is also the basis of the fast multipole method (FMM). It has been used for speeding the computation of the image-source method for monopole sources [11]. It is extended here to the case of directional sound sources.

These algorithms are applicable to calculating the sound field in a region which does not enclose any sound sources. To compute the field over a room, algorithm B must be modified slightly. since (12) only applies for interior regions where there are no sources. As shown in Figure 6, some sources lie closer to the origin than some positions of interest in the room. Equation (12) is not applicable for such sources. Assume the global origin O is in the centre of the room. Define D as the distance from O to the farthest corner of the room. For successful calculation in Algorithm B, the sound source and the one or two image-sources which lie within distance D from the centre of O must be excluded from the calculation in (12). Their contribution to the sound field can be computed separately using (11).

Algorithm B retains significant computational benefit over Algorithm A. The exclusion of some image-sources from the fast approach of Algorithm B does not subtract from its computational speed, because the number of such sound sources is so few. The computational complexity of using proposed methods is presented in the next section.

Computational Aspects

Several computational aspects of the proposed algorithms will now be discussed. Visualisation of a sound field requires sampling over a dense grid. The numbers of imagesources required for accurate simulation, depending upon the wall absorption coefficient, may also be large. Below, the numbers of grid points and image-sources required for the simulation methods are determined. The computational complexities of the two algorithms shall then be compared. A rule for whether to choose the direct Algorithm A or the two step Algorithm B is then devised.

Spatial Sampling Requirements

Consider computing the sound pressure P(x,w) over a room. Sound pressure shall be spatially sampled over a lattice of M points $x_1,...,x_M$ up to a maximum frequency f. A minimum number of lattice points is required for accurate visualization of the sound field. The largest number of spatial samples are required for frequency f for which the wavelength is $\lambda = c / f$. In a room of dimensions L_x x L_y, for visualization of a traveling wave it is reasonable to sample the field with 8 or more points per wavelength (see Figure 7). This implies sampling a N_x x N_y grid of sample points, where $N_x = [8L_x/\lambda]$ and $N_y = [8L_y/\lambda]$. The total number of pressure samples $N_p = N_x N_y$ is hence proportional to f^2.

Image-Source Numbers

There is approximately one image-source for every area of the room $A = L_x L_y$. For the T_{60} reverberation time, there are hence approximately $\pi(cT_{60})^2/A$ total imagesources for each sound source ℓ. Ignoring air absorption, T_{60} can be estimated from the wall reflection coefficient using the Sabine reverberation time [20]:

$$T_{60} = \frac{\ln 10^6}{c\bar{\alpha}} \lambda_{\text{mfp}},$$

where λ_{mfp} is the mean free path in a 2-D room given by $\lambda_{mfp} = \pi A/P$ and $P = 2(L_x+L_y)$ is the length of the room perimeter. The number of image-sources can hence be estimated as:

$$N_{\text{img}} \approx 5.92 \times 10^3 \frac{\mathscr{A}}{\mathscr{P}^2 \bar{\alpha}^2},$$

where α is the average wall absorption coefficient.

Using statistical room acoustics [20], several other useful room acoustic quantities can be obtained which are summarized in Table 2.

Table 2. Statistical room acoustic quantities for a 2-D room of area A , length of room perimeter P and average wall absorption coefficient α. Π is the radiating power of the sound source, DI is the source directivity index in the direction of interest and r is the distance from the source.

Quantity	Symbol	Equation
Reverberation time	T_{60}	$\frac{6\ln 10\pi}{c\bar{\alpha}} \frac{\mathscr{A}}{\mathscr{P}}$
Reverberant energy density	ε_r	$\frac{\pi}{c\mathscr{P}\bar{\alpha}}\Pi$
Direct energy density	ε_d	$\frac{\mathrm{DI}}{2\pi rc}\Pi$

The direct and reverberant energy densities for a sound source with radiating power P are shown. From these, the critical distance at which the direct and reverberant components are of equal energy density is:

$$r_{\text{cr}} = \frac{\mathscr{P}\bar{\alpha}\mathrm{DI}}{2\pi^2},$$

where DI is the directivity index in the source direction of interest.

Computational Complexity

The heaviest computational task involved in the imagesource method is calculating basis functions. The mode functions $H_n(kR)e^{in\Theta}$ and $J_m(kr)e^{im\Phi}$ must typically be computed over a large number of positions. An analysis of computational complexity can be based on the number of basis functions to be computed.

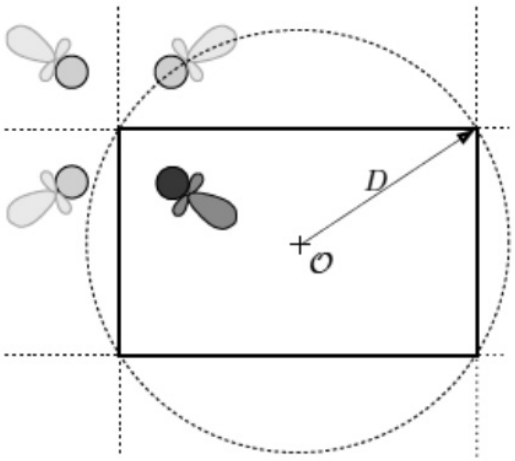

Figure 6. Shown are the direct source and an image-source lying within a circle circumscribing the room.

Algorithm A For each image-source, the sound field is computed over N_p points using the mode expansion of $2N_a+1$ terms in (5). This constitutes computed each the set of basis functions $H_m(kr^{(\ell,n)})\, e^{im\phi^{(\ell,n)}}$; $m = -N_a,\ldots,N_a$ over each of the points for a total of $N_{img}N_p(2N_a+1)$ basis function calculations for each source.

Algorithm B The modal coefficients of the sound field are first calculated in the room by determining $H_m(kR_\ell)e^{-im\Theta\ell}$ for the active modes of each imagesource. For a room of circumscribed radius D, $2N_r+1 = 2e\pi D/\lambda +1$ modes are active. For all image-sources, this totals $N_{img}(2N_r+2N_a+1)$ terms to perform the convolution. The sound field is then computed at each of N_p points by summing over the modes, requiring calculation of $(2N_r+1)N_p$ terms of $J_m(kr)e^{im\phi}$. The total is $(N_{img}+N_p)(2N_r+1)+2N_{img}N_a$ mode computations for each source.

The parameters N_a and N_r are usually dependent on frequency. At higher frequencies, the room supports more modes and a sound source has more modes of vibration.

Whilst the computation in Algorithm A is related to the product of N_{img} and N_p, for Algorithm B it is related to their sum, which may be much smaller. That is, the complexity of Algorithm A is $O(N_{img}f^3)$ while that of Algorithm B is $O(f^3)+O(N_{img}f)$.

The decision to choose Algorithm B over Algorithm A is based on the relative sizes of N_p and N_r. Based on the above reasoning, the decision rule is:

$$N_p \underset{\text{A}}{\overset{\text{B}}{\gtrless}} \frac{(2N_a+2N_r+1)N_{\text{img}}}{(2N_a+1)N_{\text{img}}-(2N_r+1)}. \qquad (14)$$

Because the total number of modes of the image-sources $N_{img}(2N_a+1)$ is usually much greater than the numbers of modes active in the room $2N_r+1$, Algorithm B is expected to be much more efficient for room simulation.

Computing the sound field for a higher order source is more time consuming than it is for an omnidirectional source. In fact, it becomes $2N_a+1$ times more timeconsuming, without the FMM-based method Algorithm B. It becomes more critical to use a multipole method for the case of directional sound sources.

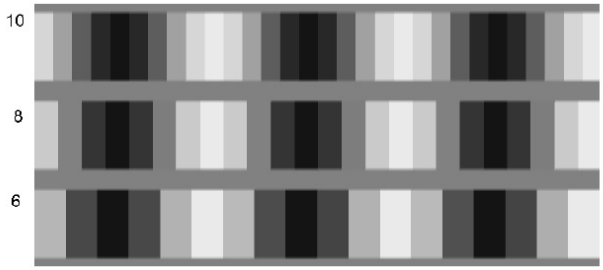

Figure 7. Plot of sine wave with 6, 8 and 10 pixels per period.

SIMULATION EXAMPLE

A single directional source shall now be simulated in a 6.4 x 5m room. Figure 8 shows the sound field at 750 Hz in the room for an acoustic monopole, a dipole and a third order pencil beam. The wall absorption coefficient here was set to 0.25 so that the influence of the source directivity pattern is clearly seen. The critical distance is 1.18 cm for a monopole, 2.36m for a dipole in the direction of the two lobes and 8.2 m for a third order beampattern in its main lobe direction. In Figure 8(a) and 8(b) the direct field dominates over the reverberant field up to the critical distance, whilst in Figure 8(c) the direct field is shown to dominate up to the room boundary.

With regard to computations aspects, to simulate in the room up to 1 kHz, at least a 150 x 120 grid of points would be recommended from above. For calculating sound pressure over this grid, the number of active modes in the room $2N_r+1$ at a frequency of 1 kHz is 204. For third order source in a room with α = 0.51, $1.77\text{x}10^8$ mode functions must be computed under Algorithm A and $7.94 \text{ x } 10^6$ mode functions must be computed under Algorithm B. To simulate omnidirectional sources in this example it is significantly more worthwhile to choose Algorithm B over Algorithm A. Applying (14), Algorithm B would still be worthwhile when the number of locations is $N_p > 239$. For directional sources, it is of even more benefit to use Algorithm B. For third order sources for example, it is worthwhile to use Algorithm B for only 31 locations.

The 2-D image-source simulator is more efficient to implement than a 3-D simulator. In 2-D, the numbers of image-sources is proportional to $(T_{60})^2$ whilst in 3-D, they are proportional to $(T_{60})^3$. In the example 2-D room, the reverberation time is 350 msec with 1400 image sources and an α of 0.51. In a 3-D room of dimensions 6.4 x 5 x 4m with the same α , the reverberation time is only 250 msec yet 28,000 image-sources are required which is an order of magnitude more.

FURTHER DISCUSSION

The 2-D method of sound field simulation is well-suited to the simulation of surround sound systems. A 2-D method is useful in particular for simulating 2.5-D surround sound systems, where both the loudspeaker and the listeners lie within the same horizontal plane [21]. Though these systems are unable to create out-of-plane sound effects, more practical numbers of loudspeaker drivers are required to control the sound field than for the 3-D case. The simulator helps establish the expected performance of surround systems in rooms.

However, due care must be taken in applying this simulation to real-world situations. By the stationary phase approximation, the 2-D model is strictly accurate in the x-y plane for sufficiently tall higher order sources. For real sources the approximation breaks down in the farfield. A key difference between 2-D and 3-D is that in 3-D the amplitude of sound pressure decays in proportion to the inverse of radius whilst in 2-D it decays according to the square root of radius [22].

The image-source method is exact for the case of a line source with perfectly rigid walls. It lends most of its application to modeling the wall absorptive cases, which it does approximately. The exact solution in this case requires a solution of the wave equation that results in complex wall reflection coefficients [20]. There are many physical other phenomena that occur in a real room not accounted for by image-source methods, including local temperature and humidity fluctuations. Yet due to its convenience, the image-source method is still commonly in use.

The image-source method is a specular reflection model. It does not account for diffuse reflections which are caused by rough surfaces. For a diffuse reflection, the angle of incidence no longer equals the angle of reflection. Instead, the sound is scattered in all directions as described by Lambert's cosine law [20, p. 81]. In [23], the image-source method was extended for diffuse reflection by replacing each image-source with a continuum of image-sources arranged on a line. In this manner, reflections are made to approximately preserve Lambert's cosine law. In future work, we shall investigate extending this approach to directional sources.

The proposed method does not model multiple scattering between cylinders. Multiple reflection of sound between closely-spaced cylinders cause interactions that cannot be modelled by a simple image-source approach. The method is thence inaccurate unless cylindrical sources are located at several cylinder radii away from walls or other cylinders for these interactions to be negligible [24]. This is not an unreasonable assumption. In the simulation of surround systems for example, it is safe to assume that loudspeakers are spaced apart. Doing so allows the system to better create spatial sound.

An alternate method to simulating the directional sources is to replace each solid source with an equivalent array of simple sources in free-space. Each cylinder could for example be replaced with a circular array of radius a of $2N_a+1$ line sources. The strength of this simulation method is that the original image-source method, which is efficiently implemented in a FMM manner [11], can be used directly. However this scheme introduces problems with inaccuracy. Circular arrays of simple sources cannot create certain sound fields. In particular, they cannot support creation of the sound field at frequencies for which the Bessel functions of ka are zero [15]. Furthermore, because of the added computation of emulating a directional source with simple sources, the method offers no computational benefit.

CONCLUSION

This paper extends the image-source method to computing the field for a set of sound sources with arbitrary directional patterns. Here the sound field is efficiently calculated over an extended area using a fast multipole method. The image-source method is applicable for multiple numbers of directional sources, provided sources are spaced several source dimensions away from other obstacles so that multiple scattering can be neglected.

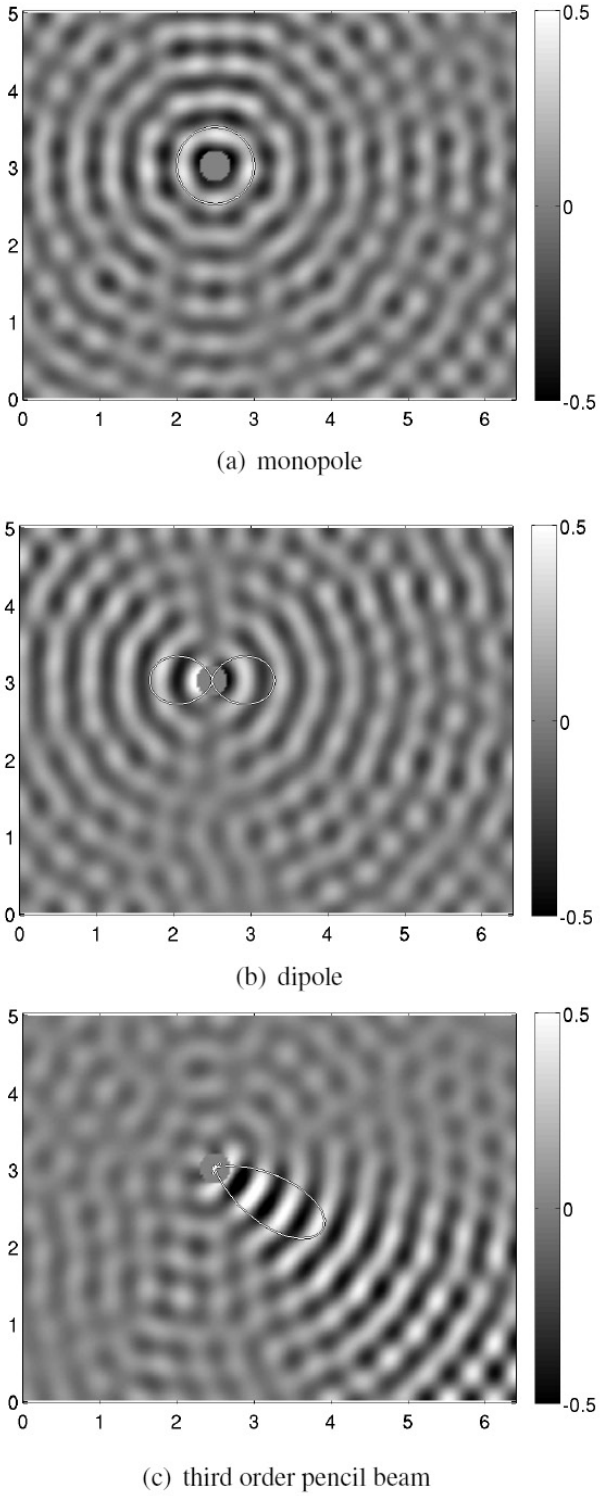

Figure 8. Sound field of a vibrating cylinder of radius a = 0.2 at 750 Hz for a (a) monopole, (b) dipole and (c) third order pencil beam in a room generated by the proposed image-source method with a 0.25 wall absorption coefficient. Far-field directivity patterns are shown.

ACKNOWLEDGEMENTS

This paper was written using funds from the New Zealand Ministry for Science and Innovation.

REFERENCES

[1] L.L. Beranek, Acoustics, Acoustical Society of America, New York, 1993.

[2] T. Holman, "Dipolar confusion: The case for dipole loudspeakers," Stereo review, 1998.

[3] K. Kowalczyk and M. Walstijn, "Wideband and isotropic room acoustics simulation using 2-D interpolated FDTD schemes," IEEE Trans. Speech and Audio Processing, vol. 18, no. 1, pp. 78–89, 2010.

[4] M. Kleiner, B. Dalenback, and P. Svensson, "Auralization -an overview," Journal of the Audio Engineering Society, vol. 41, no. 11, pp. 861–875, 1993.

[5] A. Pietrzyk, "Computer modeling of the sound field in small rooms," in Proc. of the 15th AES Int. Conf. on Audio, Acoustics and Small Spaces, 1998, vol. 2, pp. 24–31.

[6] Y. Kahana and Philip A. Nelson, "Numerical modelling of the spatial acoustic response of the human pinna," Journal of Sound and Vibration, vol. 292, no. 1, pp. 148–178, 2006.

[7] M.E. Johnson, S.J. Elliott, and K.H. Baek, "An equivalent source technique for calculating the sound field inside an enclosure containing scattering objects," J. Acoust. Soc. Am., vol. 104, no. 1, pp. 1221–1231, 1998.

[8] J. Allen and D. Berkley, "Image method for efficiently simulating small-room acoustics," Journal of the Acoustical Society of America, vol. 65, no. 4, pp. 943–950, 1979.

[9] P. Peterson, "Simulating the response of multiple microphones to a single acoustic source in a reverberant room," Journal of the Acoustical Society of America, vol. 80, no. 5, pp. 1527–1529, 1986.

[10] Eric A. Lehmann and Anders M. Johansson, "Image method for efficiently simulating small-room acoustics," Journal of the Acoustical Society of America, vol. 124, no. 269, pp. 269–278, 2008.

[11] R. Duraiswami, D. N. Zotkin, and N. A. Gumerov, "Fast evaluation of the room transfer function using multipole expansion," IEEE Transactions on Speech and Audio Processing, vol. 15, pp. 565–576, 2007.

[12] A. Wabnitz, C Jin, N. Epain, and A. Schaik, "Room acoustic simulation for multichannel microphone arrays," in Proceedings of the International Symposium on Room Acoustics (ISRA), 2010.

[13] M.A. Poletti, T.D. Abhayapala, and P. Samarasinghe, "Interior and exterior sound field control using general two dimensional higher-order variable-directivity sources," J. Acoust. Soc. Amer., vol. 129, no. 5, pp. 3814–3823, 2012. ¶